CHAPTER 7

Effect of Double Mutation (L452R and E484Q) in RBD of Spike Protein on its Interaction with ACE2 Receptor Protein

Effect of Double Mutation (L452R and E484Q) in RBD of Spike Protein on its Interaction with ACE2 Receptor Protein

7.1. Abstract:

The severe acute respiratory syndrome coronavirus-2 (SARS-CoV-2) caused coronavirus disease 2019 (COVID-19) pandemic has become a global health issue. Recently, the SARS-CoV-2 strain (B.1.617 double mutant variant) has raised alarms in India and other nations. B.1.617 variant was found to contain two key mutations (L452R and E484Q) in the RBD region of the spike protein. In this work, we have focused on the effect of the double mutations in spike protein on its binding to the host cell receptor protein, angiotensin-converting enzyme 2 (ACE2). From the MD simulation, we observed that the L452R and E484Q double mutant (DM) in spike protein utilizes unique strategies to achieve stable binding to ACE2 compared to the spike protein's wild type (WT). Using MM-GBSA/MM-PBSA algorithms, we found that the binding affinity between spike protein containing DM and ACE2 is high (GB_{TOT} = -47.09 kcal/mol, PB_{TOT} = -19.93 kcal/mol) in comparison with spike protein WT and ACE2 (GB_{TOT} =-31.79 kcal/mol, PB_{TOT} = -6.33 kcal/mol). Stable binding of spike protein to ACE2 is essential for virus entry. They should understand interactions between them while designing drugs and treatment modalities to target or disrupt this interface.

7.2. Introduction:

The ongoing spread of an infectious Coronavirus disease 2019 (COVID-19), caused by severe acute respiratory syndrome-Coronavirus-2 (SARS-CoV-2), an enveloped positive stranded RNA virus into the community, poses exceptional challenges for the healthcare system due to high incidence and long incubation time [1]. SARS-CoV-2 is a novel coronavirus isolated on January 7, 2020 [2,3] by the Chinese Center for Disease Control and Prevention. The SARS-CoV-2 spike glycoprotein (spike protein) has gained significant attention since the outbreak of the COVID-19 pandemic due to its role in viral pathogenesis and immune response [4]. As of now, the vaccines that target spike protein, being used for COVID-19, provide host cells with a genetic transcript (mRNA or adenovirus) that ribosomes translate into a mutated spike protein. However, the nature and effect of mutations on the nascent spike protein remain unclear. Spike protein is a type I transmembrane protein produced as a single-chain precursor and is subsequently processed by either furin at the trans-Golgi network [5,6] or by another proprotein convertase into a receptor-binding fragment S1 and a fusion fragment S2 [7]. After the interaction between the receptor-binding domain (RBD) of the S1 subunit with the viral receptor angiotensin I-converting enzyme 2 (ACE2), followed by a second proteolytic cleavage within S2 (S2'

site) [8-10], the spike protein experiences substantial conformational changes, causing the detachment of S1 and refolding of S2 irreversibly to form a post fusion structure [11,12]. This instigates the fusion of the virus and host cell membranes to initiate infection. Recent studies have shown that SARS-CoV-2, the coronavirus that causes COVID-19, has undergone mutations due to population transmissions and generated several variants, with new variants of the virus showing up in different places across the globe. Some of the widespread SARS-CoV-2 variants are Alpha (B.1.1.7, originally discovered in the United Kingdom), Beta (B.1.351, first discovered in South Africa), Epsilon (B.1.427 and B.1.429, first identified in United States-California), Delta (B.1.617.2, first identified in India), Gamma (P.1, first identified in Japan/Brazil). A new double mutant variant has been recently discovered in India (B.1.617). Scientists and public health officials are trying to understand the risk posed by the coronavirus variant B.1.617, which was announced a global "variant of concern (VOC)" by the World Health Organization on May 10, 2021. Variants are classified if there is evidence of their higher transmissibility, increased disease severity, or evasion of previously acquired immunity better than the circulating versions of the virus [13]. On May 7, 2021, the B.1.617.2 subtype was declared a VOC in the United Kingdom by the UK government as the confirmed B.1.617.2 infections rose from 202 to 520 in a single week in the country. In just a few weeks, the B.1.617 variant has become the dominant strain across India and has spread to about 64 nations worldwide. Since the variant was only recently designated a VOC, much research has not been done on it yet. According to WHO, preliminary studies have pointed out that the variant may spread more easily than other strains of the new coronavirus. Its role in India's unprecedented surge in COVID-19 cases is under investigation. Experts are also working towards understanding the extent of threat it presents to the rest of the world. The variant was first recognized in Maharashtra, India, on October 5, 2020, as a mutant form of the virus that causes COVID-19. Also referred to as the "double mutant", B.1.617 has acquired several mutations, including two key mutations, Leucine (452) Arginine (L452R) and Glutamic acid (484) Glutamine (E484Q), in the spike protein [14]. The mutation E484Q, was also observed in highly transmissible Brazilian and South African variants, suggesting its high infectivity. The other mutation known as L452R helps the virus evade the host's immune response. The most critical SARS-CoV-2 mutations detected worldwide have been reported in the viral spike protein, vital for the viral entry into the host cell. However, the implications of mutations on the spike protein remain unknown, and these changes may affect the 3D structure and functional behavior of the protein, especially it is binding to ACE2. Such variations can be used to pinpoint target epitopes for antibody and antiviral medication development in the fight against SARS-CoV-2 [15,16]. The two key mutations, L452R and E484Q, present in the RBD region of the spike protein may affect its binding affinity to human cell-surface protein ACE2. Modifications in the spike protein's RBD region

may lead to changes in the virus's ACE2 binding specificity and alter its antigenicity, that is, recognition by immune antibodies. Here, we seek to investigate the effect of these important mutations on SARS-CoV-2 RBD towards its binding with the ACE2 by employing MD simulation and other computational approaches.

7.3. Materials and Methods:

The initial 3-D structure of SARS-CoV-2 spike receptor-binding domain bound with ACE2 (S protein(WT)-ACE2) (PDB ID: 6lzg with a resolution of 2.50 Å) (**Figure 7.1A**) was retrieved from the Research Collaboratory for Structural Bioinformatics Protein Data bank (www.rcsb.org) [17]. The 3-D structure of the double mutant (L452R and E484Q) of SARS-CoV-2 spike receptor-binding domain bound with ACE2 (S protein(DM)-ACE2) (**Figure 7.1B**) was obtained by punctual mutation of PDB: 6lzg crystal structure using UCSF Chimera package alpha v.1.12 [18]. The energy of the double mutant complex structure was then minimized by applying steepest descents and conjugate gradient methods.

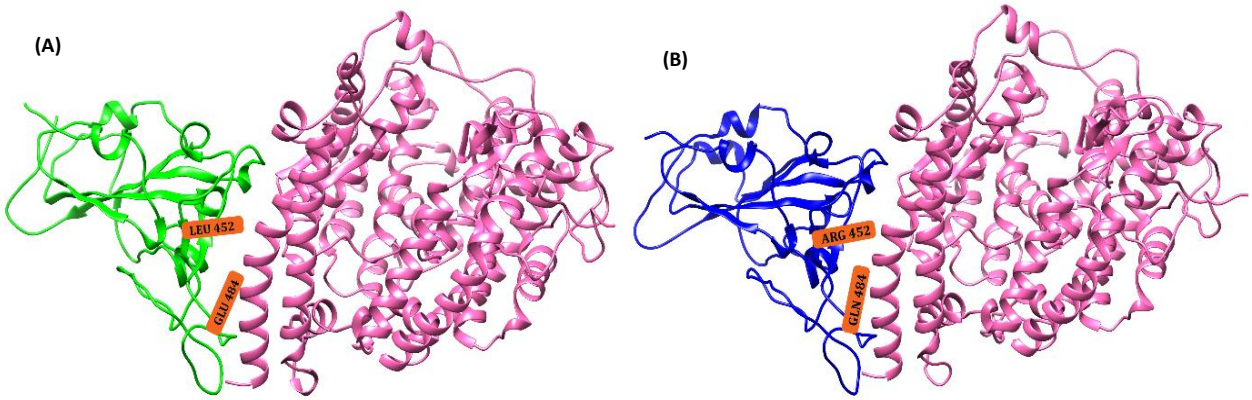

Figure 7.1. *Three-dimensional structure of* ***(A)*** *SARS-CoV-2 spike receptor-binding domain bound with ACE2 (PDB ID: 6lzg) (S protein(WT)-ACE2)* ***(B)*** *double mutant (L452R and E484Q) of SARS-CoV-2 spike receptor-binding domain bound with ACE2 (S protein (DM)-ACE2).*

7.3.1. Molecular dynamics simulations.

The wild type as well as the double mutant (L452R and E484Q) of the complex of SARS-CoV-2 spike receptor-binding domain bound with ACE2, were subjected to MD simulations. The MD simulation was performed using AMBER ff14SB force field [19,20] with AMBER software package [19]. To ensure the overall neutrality of the two complex systems, appropriate numbers of counter ions were added. MD simulations in explicit solvent were performed on the two complex systems and were solvated in all directions with TIP3P [21] water model with a solvent buffer of 10 Å [22]. In the first step of

minimization, spike receptor-binding domain and ACE2 were fixed with a 500 kcal/mol/Å^2, and minimized the energy of all water molecules and counterions for 10000 steps of steepest descents (SD) followed by 10000 steps of the conjugate gradient (CG). Subsequently, in the second step of minimization, to remove conflicting contacts, the entire complex system was repeated for 12000 steps of SD minimization and 8000 steps of CG minimization. Next, the complex system in a constant volume conditions was heated up gradually from 0-300K, thereby applying harmonic restraints with force constant of 10 kcal/mol/Å^2 on the solute atoms, and equilibration was performed three times with 3000 ps using a force constant of 5.0 kcal/mol/Å^2 [23]. Finally, 100 ns MD simulations were performed using the NPT ensemble without restraints. With the non-bonded cutoff of 12.0 Å, we applied the particle mesh Ewald [24, 25] approach of 12.0 Å to limit the direct space sum to treat the long-range electrostatic interactions. The SHAKE algorithm [26,27] was used to limit all the bonds in the system. Throughout the simulation, the Berendsen weak coupling method [28] was used to keep the pressure and temperature constant(0.5 ps of heat bath and 0.2 ps of pressure relaxation). The time step of MD simulation was set to 2 fs, and sampling was performed every 10 ps into the MD file.

The lowest energy conformer of each individual complex was identified from the highly populated clusters using the RMSD clustering algorithm after the 100 ns of production dynamics of the complexes were completed and submitted to PDBsum server to analyze for their residue-specific interactions which are considered to be important to know about the nature of interactions [29]. PDBsum [30] is a database that, among other things, shows schematic diagrams of the non-bonded contacts between amino acid residues at the interface of molecules in a multimer complex.

7.3.2. Binding free energy calculations.

The Molecular Mechanics Poisson−Boltzmann Surface Area (MM-PBSA) and Molecular Mechanics Generalized Born Surface Area (MM-GBSA) method implemented in AMBER 16 [31] package was performed to calculate the binding free energy as well as the free energy decomposition of the two complex systems (S protein(WT)-ACE2 and S protein(DM)-ACE2). For each complex system, 200 snapshots were selected from the last 10 ns of MD trajectories to calculate the relevant energies.

The formulas for calculating the BFE and their decomposed energetic components are shown in the equations (1-6). Where the total BFE (ΔG_{bind}) represents the free energy difference between the bound state complex ($G_{complex}$) and the free state individuals of the receptor ($G_{receptor}$) and ligand (G_{ligand}). According to the second law of thermodynamics, ΔGbind can be decomposed into enthalpy (ΔH) and entropy (TΔS). Poisson–Boltzmann or Generalized-Born surface area continuum solvation (MM-

PBSA/MM-GBSA) method [32,33], and normal mode (nmode) analysis [31] were used to determine the enthalpies and the entropy of the complexes respectively. After collecting all of the trajectories for MM-PBSA/MM-GBSA calculations, the three components of the individual two complexes were analysed: (i) ligand (S protein), (ii) receptor (ACE2), and (iii) complex (S protein-ACE2). Many recent in-silico investigations have employed the methodologies and protocols that we explored in this study to estimate the binding free energy [34,35].

BFE for the two complex systems was calculated using **Equation (1):**

$$\Delta G_{binding} = \Delta G_{complex} - [\Delta G_{receptor} + \Delta G_{ligand}] \quad (1)$$

where, $\Delta G_{binding}$ is the total binding free energy.

Thermodynamically,

$$\Delta G = \Delta H - T\Delta S \quad (2)$$

$$\Delta G = \Delta E_{MM} + \Delta G_{sol} - T\Delta S \quad (3)$$

$$\Delta E_{MM} = \Delta E_{int} + \Delta E_{ele} + \Delta E_{vdw} \quad (4)$$

and

$$\Delta G_{sol} = \Delta G_{PB/GB} + \Delta G_{SURF} \quad (5)$$

$$\Delta G_{SURF} = ENP + E_{dis} \quad (6)$$

Enthalpy calculations with MM-GBSA/PBSA: As shown in the **Equation (1),** for the two complex systems (S protein(WT)-ACE2 and S protein(DM)-ACE2), $\Delta G_{complex}$, $\Delta G_{receptor}$ and ΔG_{ligand} represent free energy contributions from S protein-ACE2 (complex), ACE2 (receptor) and S protein (ligand) respectively.

The enthalpy part is calculated by summation of change in molecular mechanics components in the gas phase (ΔE_{MM}) and the stabilization energy due to solvation (ΔG_{sol}) as shown in **Equation (3).** ΔE_{MM} represents the summation of internal energy (ΔE_{int}) (bond, angle, and dihedral energies), electrostatic interaction (ΔE_{ele}), and van der Waals interaction (ΔE_{vdw}). The solvation free energy (ΔGsol) is divided into electrostatic solvation free energy ($\Delta G_{PB/GB}$) and the non-polar solvation free energy (ΔG_{SURF}) contribution as shown in **Equation (5).** $\Delta G_{PB/GB}$ is calculated by Poisson-Boltzmann/Generalized-Boltzmann models and ΔG_{SURF}, the summation of non-polar contribution calculated by PB (ENP) and dispersion energy (E_{dis}) using Solvent accessibility surface area (SASA). Energy decompositions were performed to identify the important residues within the two complex systems. Here, only per-residue decomposition was included, which was used to separate the energy

contribution of each residue from the combination of Protein (ACE2) with the ligand (S protein) into three terms: van der Waals contribution (ΔE_{vdW}), electrostatic contribution (ΔE_{ele}), and solvation contribution ($\Delta GGB + \Delta GSA$).

7.4. Results and Discussion:

During May 2021, India has faced the world's most devastating wave of coronavirus infections since the start of the COVID-19 pandemic. The situation remained grim as the country records a staggering number of daily new infections at around four lakh. Despite the pain and suffering, scientists are working round the clock to identify the reason for such a 'tsunami' of the cases. And one of the main suspects remains the emergence of the more virulent mutant variants of the coronavirus. Recently, the Indian SARS-CoV-2 Genomics Consortium revealed that India's two most prevalent variants are the UK variant (B.1.1.7) and the double mutant variant from India (B.1.617). The new double mutant variant from India carries the genetic code from two other mutations, E484Q and L452R, which were already circulating globally. While both the mutations, traced across separate variants, are characteristic for their high infectivity and transmission rates, this is the first time they have merged, making it many times more infectious and deadly. The double mutations in this variant are expected, therefore, to develop resistance to antibodies that are generated by vaccination or by natural infection. However, the impact of this newly reported variant has not yet been investigated. Here, we performed a computational study to investigate the effect of these mutations on the binding affinity of spike protein for ACE2 and its impact on transmission.

7.4.1. MD simulation.

The RBD domain of wild-type strain of COVID-19 has been explored, and the structure of this SARS-CoV-2 spike receptor-binding domain bound with ACE2 protein has been reported. From the wild type structure of SARS-CoV-2 spike receptor-binding domain bound with ACE2 (S protein(WT)-ACE2), the 3-D structure of the double mutant (L452R and E484Q) of SARS-CoV-2 spike receptor-binding domain bound with ACE2 (S protein(DM)-ACE2) was obtained by punctual mutation. Then the energy minimization was carried out on the double mutant complex structure using steepest descents followed by conjugate gradient minimization. Both the complexes were then subjected to AMBER program for performing MD simulation .

7.4.1.1. RMSD analysis.

To test the stability of the (S protein(WT)-ACE2) and (S protein(DM)-ACE2) complexes, 100 ns of MD simulation studies were carried out. The conformational snapshots of the (S protein(WT)-ACE2) and (S protein(DM)-ACE2) complexes during the course of 100 ns MD simulation time were depicted in **Figure 7.2 and Figure 7.3.**

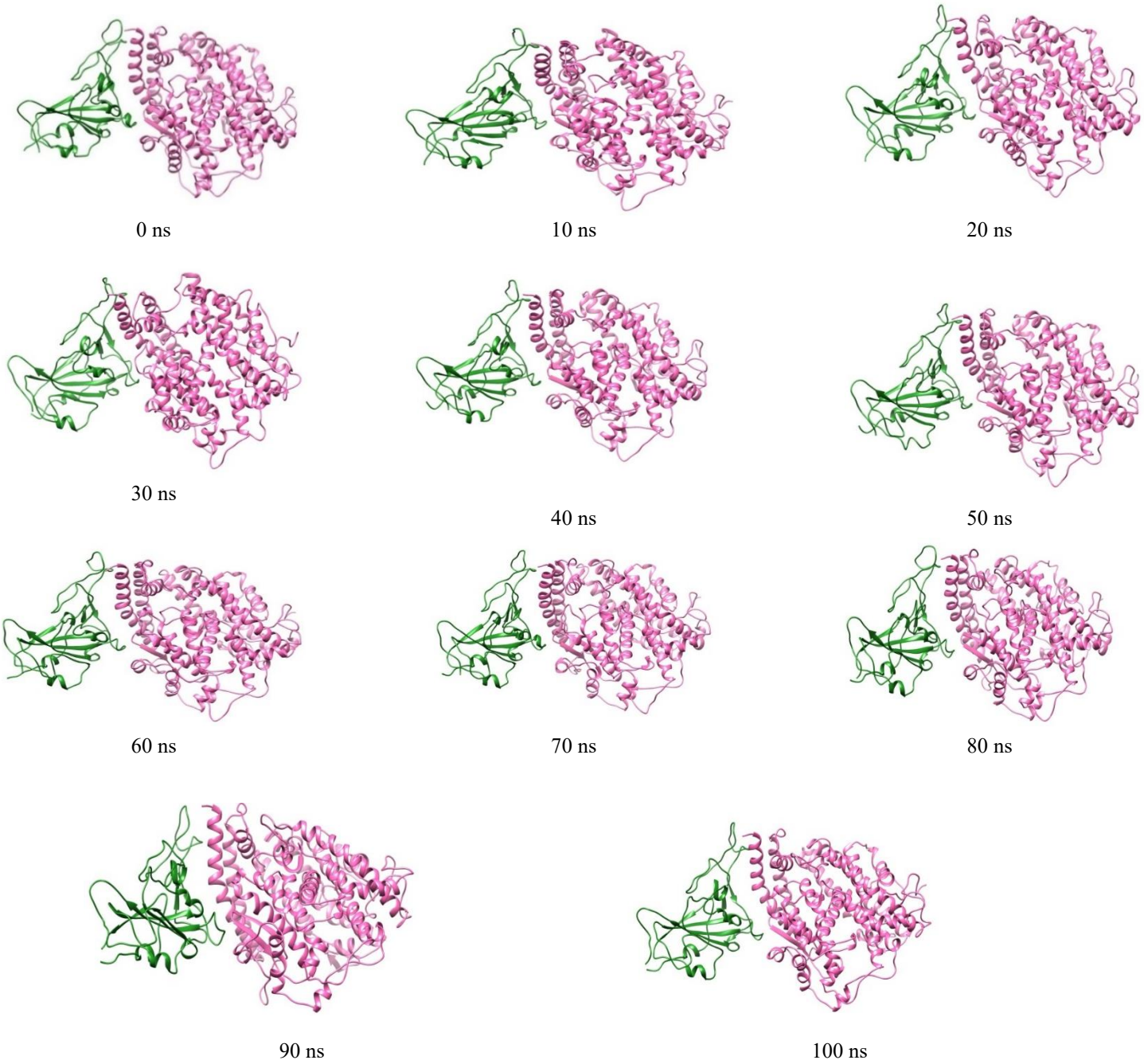

Figure 7.2. *Conformational snapshots of S protein (WT)-ACE2 complex at the time interval of 10 ns during the course of 100 ns MD simulation*

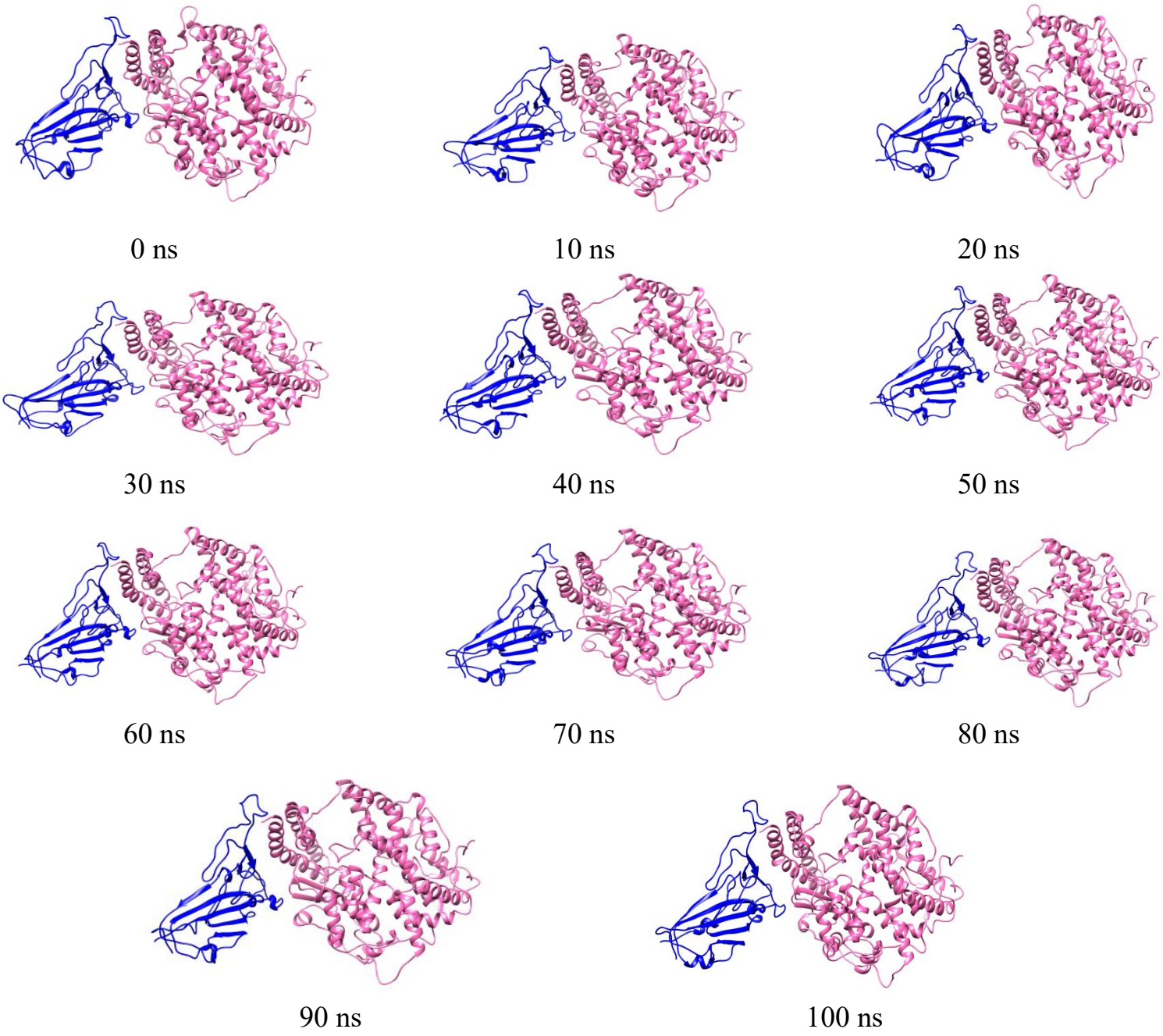

Figure 7.3. *Conformational snapshots of S protein (DM)-ACE2 complex at the time interval of 10 ns during the course of 100 ns of MD simulation*

The average deviations in atomic locations and stability throughout a 100-ns trajectory of the MD simulations, as well as the RMSD values of the complex's backbone atoms along with the S protein (apo form) were calculated. (**Figure 7.4**). The RMSD of wild type and the double mutant complex appeared to be stable after 10 ns, revealing that good convergence was achieved for each system. Interestingly, we noticed that the RMSD of the double mutant complex was slightly smaller than that of the wild-type complex. The average of RMSD is 1.84 Å (± 0.12) for the wild type complex structure and 1.42 Å (± 0.14) for the double mutant complex structure, which could indicate greater stability of the mutated complex structure. We have also compared the average deviations in the atomic positions of the residues exclusively at the mutation sites 452 and 484 (**Figure 7.5**). At residue index 452, wild-type and mutant complexes showed a similar profile in the RMSD values. In contrast, at residue index 484, compared to the mutant, wild type indicated slightly higher RMSD values in the latter portion of 100 ns MD simulation. We also noticed that the binding of ACE2 reduced the perturbation of S protein to a significant extent in both wild-type and complex mutant systems.

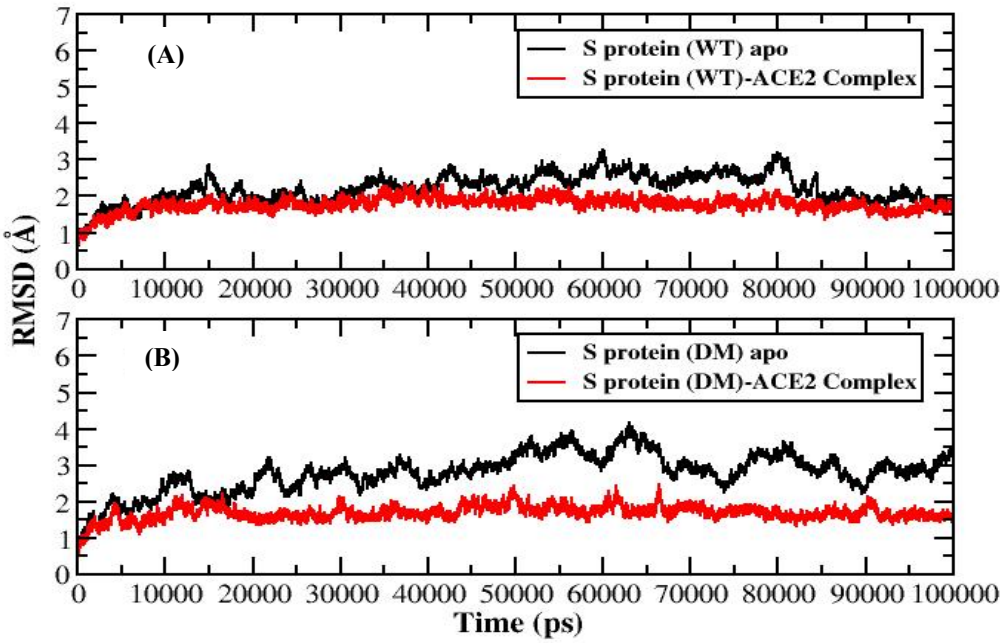

***Figure 7.4**. Backbone RMSD's for **(A)** S protein (WT) apo (black), S protein (WT)-ACE2 complex (red) **(B)** S protein (DM) apo (black), S protein (DM)-ACE2 complex (red).*

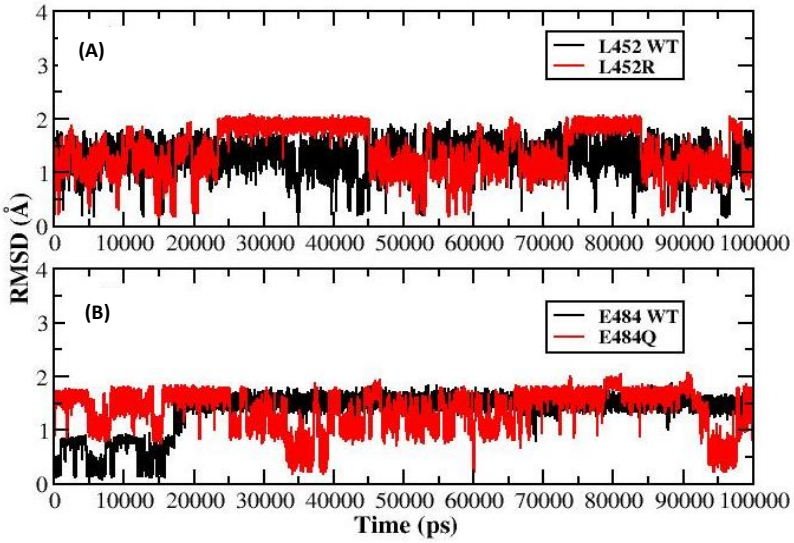

Figure 7.5. *RMSD plot of the residue at position* ***(A)*** *452* ***(B)*** *484 in the S protein (WT)-ACE2 complex (black) and S protein (DM)-ACE2 complex (red).*

7.4.1.2. RMSF analysis.

We further explored the S protein flexibility by RMSF values of the Cα from the MD simulations of the (S protein (WT)-ACE2) and (S protein (DM)-ACE2) complexes (**Figure 7.6**). We observed significant differences in the flexibility of S protein in wild type and mutant complex, particularly at the region in and around the mutation position (452 and 484). The RMSF values for the wild and mutant residue at position 452 were 4.67 Å, and 2.35 Å while at position 484 were 4.85 Å and 2.40 Å respectively in the wild type and mutant complexes, which confirms the reduction of structural fluctuations in the mutation position and increased stability.

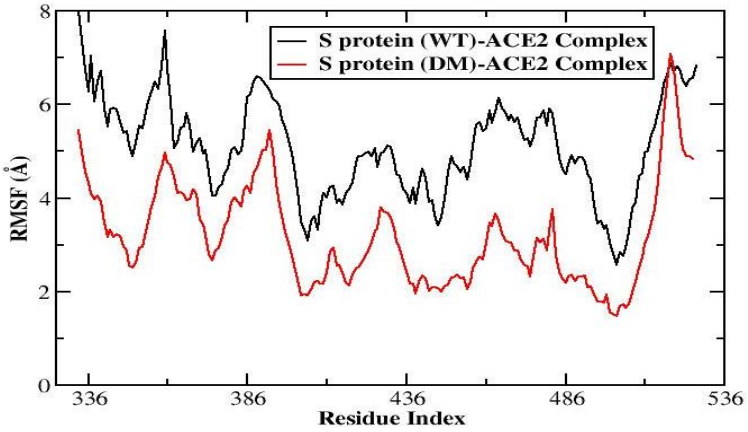

Figure 7.6. *Backbone RMSF's for S protein in* ***(A)*** *S protein (WT)-ACE2 complex (black)* ***(B)*** *S protein (DM)-ACE2 complex (red).*

7.4.1.3. Hydrogen bond analysis.

The number of hydrogen bonds present were also calculated for the (S protein(WT)-ACE2) and (S protein(DM)-ACE2) complexes (**Figure 7.7**), as these hydrogen bonds play a crucial role in conferring the stability to the protein complexes. The number of intermolecular hydrogen bonds was found to be higher in S protein(DM)-ACE2 complex than in S protein(WT)-ACE2 complex.

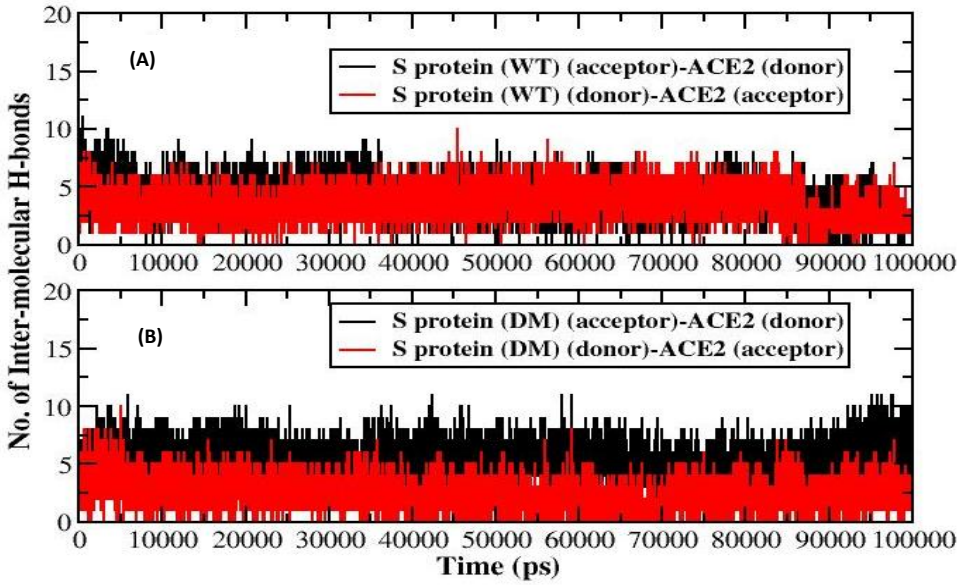

Figure 7.7. *Number of intermolecular hydrogen bonds between S protein and ACE2 in* ***(A)*** *S protein (WT)-ACE2 complex* ***(B)*** *S protein (DM)-ACE2 complex.*

7.4.1.4. Determination of the interface interactions of the S protein(WT)-ACE2) and (S protein(DM)-ACE2 complexes.

A region where two sets of proteins come into contact with each other is commonly refered to as an interface area. Surface residues with significant surface areas that are exposed to the solvent are frequently characterised. The interface statistics for the S protein(WT)-ACE2 and S protein(DM)-ACE2 complexes were obtained upon submitting the corresponding lowest energy structure extracted from the 100 ns MD simulation trajectory using RMSD clustering algorithm the PDBsum server. The interface statistics for both complexes have been shown in **Table 7.1.**

Table 7.1. *Interface statistics for the S protein(WT)-ACE2 and S protein(DM)-ACE2* complexes.

Complex system	Chain	No. of interface residues	Interface area (Å^2)	No. of salt bridges	No. of disulphide bonds	No. of hydrogen bonds	No. of non-bonded contacts
S protein (WT)-ACE2	ACE2	20	854	1	-	8	115
	S protein (WT)	19	907				
S protein (DM)-ACE2	ACE2	20	982	1	-	13	197
	S protein (DM)	20	1004				

The summarized intermolecular interactions between S protein and ACE2 of the wild type and mutant complexes at the residue levels were shown in **Figure 7.8**.

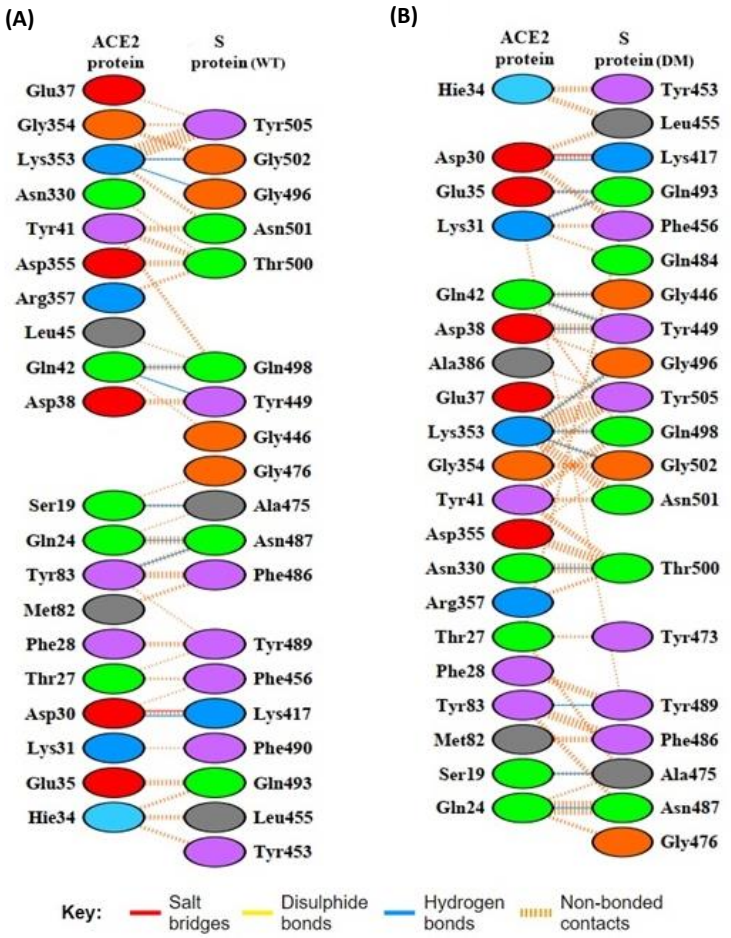

Figure 7.8. *Intermolecular interactions at residue level between ACE2 and S protein in* ***(A)*** *S protein(WT)-ACE2 and* ***(B)*** *S protein(DM)-ACE2 complexes.*

The detailed contributions of each interface residue stabilizing the wild type and mutant complexes were summarized in **Tables 7.2-7.7**. The total number of interface residues in the S protein(WT)-ACE2 and S protein(DM)-ACE2 complexes were found to be thirty-nine and forty respectively. In the S protein(WT)-ACE2 complex, the interface area involved in the interaction of the S protein and the ACE2 chain was observed to be 907 $Å^2$ and 854 $Å^2$, respectively, while in the S protein(DM)-ACE2 complex, the S protein chain and the ACE2 chain involved in the interaction was observed to be 1004 $Å^2$ and 982 $Å^2$ respectively. Molecular interactions like salt bridges, hydrogen bonding, and non-bonded contacts stabilised the wild-type and mutant type complexes.

From **Table 7.2 -7.7** we can see the presence of one hundred and fifteen non-bonded contacts, one salt bridge, and eight hydrogen bonds at the interface of S protein and ACE2 in the S protein(WT)-ACE2 complex. However, at the interface of S protein and ACE2 in the S protein(DM)-ACE2 complex, we observed one hundred and ninety-seven non-bonded contacts, one salt bridge and thirteen hydrogen bonds. An increase in the number of hydrogen bonds between the S protein and ACE2 from eight to thirteen can be seen in the S protein(DM)-ACE2 complex. Compared to the S protein(WT)-ACE2 complex, six hydrogen bonds were preserved in the S protein(DM)-ACE2 complex. In the S protein(DM)-ACE2 complex structure, we have observed the formation of seven additional hydrogen bonds between residues: Glu35-Gln493, Lys31-Gln493, Gln42-Gly446, Asp38-Tyr449, Lys353-Gln498, Asn330-Thr500, including one between Tyr83-Tyr489, having π-π interaction.

Overall, we see the number of intermolecular interactions and the interface area shared by S protein and ACE2 in forming complex is larger in mutant complex than in the wild type complex. Therefore the stability of the mutant complex was found to be higher than the wild-type complex.

***Table 7.2**. List of atom-atom interactions (Hydrogen bonds) across protein-protein interface in S protein (WT)–ACE2 complex from PDBsum server*

ACE2						Hydrogen bonds	S protein (WT)					
Sl.no.	Atom no.	Atom name	Res name	Res no.	Chain		Atom no.	Atom name	Res name	Res no.	Chain	Distance
1	10	OG	SER	19	A	<-->	11754	O	ALA	475	B	2.81
2	89	NE2	GLN	24	A	<-->	11898	OD1	ASN	487	B	2.87
3	188	OD2	ASP	30	A	<-->	10810	NZ	LYS	417	B	2.86
4	387	OE1	GLN	42	A	<-->	11286	OH	TYR	449	B	3.09
5	387	OE1	GLN	42	A	<-->	12076	NE2	GLN	498	B	3.22
6	1015	OH	TYR	83	A	<-->	11899	ND2	ASN	487	B	2.82
7	5306	O	LYS	353	A	<-->	12123	N	GLY	502	B	2.79
8	5301	NZ	LYS	353	A	<-->	12043	O	GLY	496	B	3.22

Table 7.3. *List of atom-atom interactions (non-bonded) across protein-protein interface in S protein (WT)–ACE2 complex from PDBsum server*

ACE2						Non-bonded	S protein (WT)					
Sl.no.	Atom no.	Atom name	Res name	Res no.	Chain		Atom no.	Atom name	Res name	Res no.	Chain	Distance
1	7	CB	SER	19	A	<-->	11754	O	ALA	475	B	3.62
2	10	OG	SER	19	A	<-->	11753	C	ALA	475	B	3.89
3	10	OG	SER	19	A	<-->	11754	O	ALA	475	B	2.81
4	10	OG	SER	19	A	<-->	11757	CA	GLY	476	B	3.81
5	81	CB	GLN	24	A	<-->	11899	ND2	ASN	487	B	3.82
6	84	CG	GLN	24	A	<-->	11754	O	ALA	475	B	3.89
7	84	CG	GLN	24	A	<-->	11897	CG	ASN	487	B	3.48
8	84	CG	GLN	24	A	<-->	11898	OD1	ASN	487	B	3.25
9	84	CG	GLN	24	A	<-->	11899	ND2	ASN	487	B	3.24
10	87	CD	GLN	24	A	<-->	11898	OD1	ASN	487	B	3.38
11	89	NE2	GLN	24	A	<-->	11897	CG	ASN	487	B	3.83
12	89	NE2	GLN	24	A	<-->	11898	OD1	ASN	487	B	2.87
13	139	O	THR	27	A	<-->	11424	CZ	PHE	456	B	3.77
14	132	CG2	THR	27	A	<-->	11422	CE1	PHE	456	B	3.53
15	132	CG2	THR	27	A	<-->	11929	CE2	TYR	489	B	3.62
16	140	N	PHE	28	A	<-->	11927	OH	TYR	489	B	3.83
17	142	CA	PHE	28	A	<-->	11927	OH	TYR	489	B	3.36
18	144	CB	PHE	28	A	<-->	11927	OH	TYR	489	B	3.4
19	148	CD1	PHE	28	A	<-->	11927	OH	TYR	489	B	3.84
20	183	CB	ASP	30	A	<-->	11422	CE1	PHE	456	B	3.87
21	186	CG	ASP	30	A	<-->	10810	NZ	LYS	417	B	3.61
22	187	OD1	ASP	30	A	<-->	10810	NZ	LYS	417	B	3.76
23	188	OD2	ASP	30	A	<-->	10810	NZ	LYS	417	B	2.86
24	207	NZ	LYS	31	A	<-->	11954	O	PHE	490	B	3.82
25	251	CB	HIE	34	A	<-->	12000	NE2	GLN	493	B	3.53
26	254	CG	HIE	34	A	<-->	11361	OH	TYR	453	B	3.72
27	255	ND1	HIE	34	A	<-->	11402	CD1	LEU	455	B	3.71
28	256	CE1	HIE	34	A	<-->	11402	CD1	LEU	455	B	3.34
29	258	NE2	HIE	34	A	<-->	11361	OH	TYR	453	B	3.79
30	258	NE2	HIE	34	A	<-->	11402	CD1	LEU	455	B	3.37
31	260	CD2	HIE	34	A	<-->	11361	OH	TYR	453	B	2.93
32	260	CD2	HIE	34	A	<-->	11402	CD1	LEU	455	B	3.8
33	262	C	HIE	34	A	<-->	12000	NE2	GLN	493	B	3.53
34	263	O	HIE	34	A	<-->	12000	NE2	GLN	493	B	3.52
35	264	N	GLU	35	A	<-->	12000	NE2	GLN	493	B	3.77
36	274	CD	GLU	35	A	<-->	12000	NE2	GLN	493	B	3.77
37	275	OE1	GLU	35	A	<-->	12000	NE2	GLN	493	B	3.39
38	276	OE2	GLU	35	A	<-->	11999	OE1	GLN	493	B	3.68
39	276	OE2	GLU	35	A	<-->	12000	NE2	GLN	493	B	3.87

40	301	OE2	GLU	37	A	<-->	12166	OH	TYR	505	B	3.66
41	311	CG	ASP	38	A	<-->	11286	OH	TYR	449	B	3.55
42	312	OD1	ASP	38	A	<-->	11286	OH	TYR	449	B	3.51
43	313	OD2	ASP	38	A	<-->	11288	CE2	TYR	449	B	3.57
44	313	OD2	ASP	38	A	<-->	11285	CZ	TYR	449	B	3.65
45	313	OD2	ASP	38	A	<-->	11286	OH	TYR	449	B	2.83
46	372	CD2	TYR	41	A	<-->	12075	OE1	GLN	498	B	3.85
47	365	CE1	TYR	41	A	<-->	12118	ND2	ASN	501	B	3.88
48	370	CE2	TYR	41	A	<-->	12074	CD	GLN	498	B	3.86
49	370	CE2	TYR	41	A	<-->	12075	OE1	GLN	498	B	3.88
50	370	CE2	TYR	41	A	<-->	12118	ND2	ASN	501	B	3.46
51	367	CZ	TYR	41	A	<-->	12105	OG1	THR	500	B	3.85
52	367	CZ	TYR	41	A	<-->	12118	ND2	ASN	501	B	3.21
53	368	OH	TYR	41	A	<-->	12107	C	THR	500	B	3.43
54	368	OH	TYR	41	A	<-->	12108	O	THR	500	B	3.51
55	368	OH	TYR	41	A	<-->	12099	CB	THR	500	B	3.46
56	368	OH	TYR	41	A	<-->	12105	OG1	THR	500	B	2.73
57	368	OH	TYR	41	A	<-->	12109	N	ASN	501	B	3.62
58	368	OH	TYR	41	A	<-->	12118	ND2	ASN	501	B	3.11
59	386	CD	GLN	42	A	<-->	12076	NE2	GLN	498	B	3.73
60	387	OE1	GLN	42	A	<-->	11251	O	GLY	446	B	3.34
61	387	OE1	GLN	42	A	<-->	11286	OH	TYR	449	B	3.09
62	387	OE1	GLN	42	A	<-->	12074	CD	GLN	498	B	3.85
63	387	OE1	GLN	42	A	<-->	12075	OE1	GLN	498	B	3.64
64	387	OE1	GLN	42	A	<-->	12076	NE2	GLN	498	B	3.22
65	388	NE2	GLN	42	A	<-->	12076	NE2	GLN	498	B	3.6
66	428	CD2	LEU	45	A	<-->	12076	NE2	GLN	498	B	3.57
67	989	CB	MET	82	A	<-->	11880	CE1	PHE	486	B	3.63
68	995	SD	MET	82	A	<-->	11878	CD1	PHE	486	B	3.66
69	995	SD	MET	82	A	<-->	11880	CE1	PHE	486	B	3.75
70	1012	CE1	TYR	83	A	<-->	11882	CZ	PHE	486	B	3.79
71	1012	CE1	TYR	83	A	<-->	11899	ND2	ASN	487	B	3.86
72	1017	CE2	TYR	83	A	<-->	11880	CE1	PHE	486	B	3.79
73	1014	CZ	TYR	83	A	<-->	11880	CE1	PHE	486	B	3.48
74	1014	CZ	TYR	83	A	<-->	11882	CZ	PHE	486	B	3.69
75	1014	CZ	TYR	83	A	<-->	11899	ND2	ASN	487	B	3.79
76	1015	OH	TYR	83	A	<-->	11880	CE1	PHE	486	B	3.33
77	1015	OH	TYR	83	A	<-->	11882	CZ	PHE	486	B	3.69
78	1015	OH	TYR	83	A	<-->	11897	CG	ASN	487	B	3.65
79	1015	OH	TYR	83	A	<-->	11899	ND2	ASN	487	B	2.82
80	1015	OH	TYR	83	A	<-->	11927	OH	TYR	489	B	3.54
81	4963	OD1	ASN	330	A	<-->	12101	CG2	THR	500	B	3.53
82	5287	CA	LYS	353	A	<-->	12160	CG	TYR	505	B	3.61
83	5287	CA	LYS	353	A	<-->	12161	CD1	TYR	505	B	3.63
84	5287	CA	LYS	353	A	<-->	12170	CD2	TYR	505	B	3.72

85	5287	CA	LYS	353	A	<-->	12163	CE1	TYR	505	B	3.76
86	5287	CA	LYS	353	A	<-->	12168	CE2	TYR	505	B	3.85
87	5287	CA	LYS	353	A	<-->	12165	CZ	TYR	505	B	3.86
88	5305	C	LYS	353	A	<-->	12160	CG	TYR	505	B	3.67
89	5305	C	LYS	353	A	<-->	12161	CD1	TYR	505	B	3.37
90	5305	C	LYS	353	A	<-->	12163	CE1	TYR	505	B	3.77
91	5306	O	LYS	353	A	<-->	12111	CA	ASN	501	B	3.58
92	5306	O	LYS	353	A	<-->	12121	C	ASN	501	B	3.66
93	5306	O	LYS	353	A	<-->	12113	CB	ASN	501	B	3.68
94	5306	O	LYS	353	A	<-->	12123	N	GLY	502	B	2.79
95	5306	O	LYS	353	A	<-->	12125	CA	GLY	502	B	3.68
96	5306	O	LYS	353	A	<-->	12157	CB	TYR	505	B	3.56
97	5306	O	LYS	353	A	<-->	12160	CG	TYR	505	B	3.59
98	5306	O	LYS	353	A	<-->	12161	CD1	TYR	505	B	3.51
99	5289	CB	LYS	353	A	<-->	12170	CD2	TYR	505	B	3.88
100	5292	CG	LYS	353	A	<-->	12170	CD2	TYR	505	B	3.75
101	5301	NZ	LYS	353	A	<-->	12043	O	GLY	496	B	3.22
102	5307	N	GLY	354	A	<-->	12161	CD1	TYR	505	B	3.78
103	5307	N	GLY	354	A	<-->	12163	CE1	TYR	505	B	3.88
104	5312	C	GLY	354	A	<-->	12123	N	GLY	502	B	3.69
105	5312	C	GLY	354	A	<-->	12125	CA	GLY	502	B	3.87
106	5313	O	GLY	354	A	<-->	12123	N	GLY	502	B	3.61
107	5313	O	GLY	354	A	<-->	12125	CA	GLY	502	B	3.45
108	5318	CB	ASP	355	A	<-->	12108	O	THR	500	B	3.8
109	5321	CG	ASP	355	A	<-->	12108	O	THR	500	B	3.54
110	5323	OD2	ASP	355	A	<-->	12108	O	THR	500	B	3.36
111	5323	OD2	ASP	355	A	<-->	12099	CB	THR	500	B	3.75
112	5323	OD2	ASP	355	A	<-->	12105	OG1	THR	500	B	3.86
113	5365	NH2	ARG	357	A	<-->	12099	CB	THR	500	B	3.43
114	5365	NH2	ARG	357	A	<-->	12105	OG1	THR	500	B	3.66
115	5365	NH2	ARG	357	A	<-->	12101	CG2	THR	500	B	3.57

***Table 7.4**. List of atom-atom interactions (salt bridges) across protein-protein interface in S protein (WT)–ACE2 complex from PDBsum server*

ACE2						**salt bridges**	**S protein (WT)**					
Sl.no.	Atom no.	Atom name	Res name	Res no.	Chain		Atom no.	Atom name	Res name	Res no.	Chain	Distance
1	187	OD1	ASP	30	A	<-->	10810	NZ	LYS	417	B	2.86

***Table 7.5**. List of atom-atom interactions (Hydrogen bonds) across protein-protein interface in S protein (DM)–ACE2 complex from PDBsum server*

ACE2							S protein (WT)					
Sl.no.	Atom no.	Atom name	Res name	Res no.	Chain	**Hydrogen bonds**	Atom no.	Atom name	Res name	Res no.	Chain	Distance
1	1	N	SER	19	A	<-->	11759	O	ALA	475	B	2.59
2	88	OE1	GLN	24	A	<-->	11906	ND2	ASN	487	B	2.52
3	188	OD2	ASP	30	A	<-->	10810	NZ	LYS	417	B	2.52
4	207	NZ	LYS	31	A	<-->	12006	OE1	GLN	493	B	2.6
5	275	OE1	GLU	35	A	<-->	12007	NE2	GLN	493	B	2.61
6	313	OD2	ASP	38	A	<-->	11286	OH	TYR	449	B	2.29
7	388	NE2	GLN	42	A	<-->	11251	O	GLY	446	B	2.52
8	388	NE2	GLN	42	A	<-->	11286	OH	TYR	449	B	2.68
9	1015	OH	TYR	83	A	<-->	11934	OH	TYR	489	B	2.83
10	4964	ND2	ASN	330	A	<-->	12115	O	THR	500	B	3.17
11	5306	O	LYS	353	A	<-->	12130	N	GLY	502	B	2.81
12	5301	NZ	LYS	353	A	<-->	12050	O	GLY	496	B	2.52
13	5301	NZ	LYS	353	A	<-->	12082	OE1	GLN	498	B	2.72

***Table 7.6**. List of atom-atom interactions (non-bonded) across protein-protein interface in S protein (DM)–ACE2 complex from PDBsum server*

ACE2							S protein (WT)					
Sl.no.	Atom no.	Atom name	Res name	Res no.	Chain	**non-bonded**	Atom no.	Atom name	Res name	Res no.	Chain	Distance
1	1	N	SER	19	A	<-->	11758	C	ALA	475	B	3.81
2	1	N	SER	19	A	<-->	11759	O	ALA	475	B	2.59
3	5	CA	SER	19	A	<-->	11759	O	ALA	475	B	3.87
4	79	CA	GLN	24	A	<-->	11905	OD1	ASN	487	B	3.68
5	81	CB	GLN	24	A	<-->	11904	CG	ASN	487	B	3.63
6	81	CB	GLN	24	A	<-->	11905	OD1	ASN	487	B	2.86
7	81	CB	GLN	24	A	<-->	11906	ND2	ASN	487	B	3.57
8	84	CG	GLN	24	A	<-->	11758	C	ALA	475	B	3.76
9	84	CG	GLN	24	A	<-->	11759	O	ALA	475	B	3.32
10	84	CG	GLN	24	A	<-->	11762	CA	GLY	476	B	3.82
11	84	CG	GLN	24	A	<-->	11904	CG	ASN	487	B	3.63
12	84	CG	GLN	24	A	<-->	11905	OD1	ASN	487	B	2.74
13	84	CG	GLN	24	A	<-->	11906	ND2	ASN	487	B	3.79
14	87	CD	GLN	24	A	<-->	11762	CA	GLY	476	B	3.62
15	87	CD	GLN	24	A	<-->	11904	CG	ASN	487	B	3.57
16	87	CD	GLN	24	A	<-->	11905	OD1	ASN	487	B	3.11
17	87	CD	GLN	24	A	<-->	11906	ND2	ASN	487	B	3.4
18	88	OE1	GLN	24	A	<-->	11904	CG	ASN	487	B	3.06
19	88	OE1	GLN	24	A	<-->	11905	OD1	ASN	487	B	3.03

20	88	OE1	GLN	24	A	<-->	11906	ND2	ASN	487	B	2.52
21	89	NE2	GLN	24	A	<-->	11762	CA	GLY	476	B	3.67
22	139	O	THR	27	A	<-->	11429	CZ	PHE	456	B	3.53
23	130	CB	THR	27	A	<-->	11754	CB	ALA	475	B	3.73
24	136	OG1	THR	27	A	<-->	11754	CB	ALA	475	B	3.87
25	132	CG2	THR	27	A	<-->	11427	CE1	PHE	456	B	3.75
26	132	CG2	THR	27	A	<-->	11729	CD2	TYR	473	B	3.74
27	132	CG2	THR	27	A	<-->	11727	CE2	TYR	473	B	3.6
28	132	CG2	THR	27	A	<-->	11754	CB	ALA	475	B	3.76
29	142	CA	PHE	28	A	<-->	11934	OH	TYR	489	B	3.89
30	144	CB	PHE	28	A	<-->	11933	CZ	TYR	489	B	3.88
31	144	CB	PHE	28	A	<-->	11934	OH	TYR	489	B	3.3
32	147	CG	PHE	28	A	<-->	11934	OH	TYR	489	B	3.63
33	148	CD1	PHE	28	A	<-->	11933	CZ	TYR	489	B	3.9
34	148	CD1	PHE	28	A	<-->	11934	OH	TYR	489	B	3.24
35	190	O	ASP	30	A	<-->	11411	CD2	LEU	455	B	3.7
36	183	CB	ASP	30	A	<-->	11427	CE1	PHE	456	B	3.83
37	186	CG	ASP	30	A	<-->	10807	CE	LYS	417	B	3.61
38	186	CG	ASP	30	A	<-->	10810	NZ	LYS	417	B	3.32
39	186	CG	ASP	30	A	<-->	11427	CE1	PHE	456	B	3.8
40	187	OD1	ASP	30	A	<-->	10807	CE	LYS	417	B	3.23
41	187	OD1	ASP	30	A	<-->	10810	NZ	LYS	417	B	3.48
42	188	OD2	ASP	30	A	<-->	10807	CE	LYS	417	B	3.26
43	188	OD2	ASP	30	A	<-->	10810	NZ	LYS	417	B	2.52
44	188	OD2	ASP	30	A	<-->	11405	CG	LEU	455	B	3.27
45	188	OD2	ASP	30	A	<-->	11407	CD1	LEU	455	B	3.24
46	188	OD2	ASP	30	A	<-->	11411	CD2	LEU	455	B	3.6
47	188	OD2	ASP	30	A	<-->	11425	CD1	PHE	456	B	3.72
48	188	OD2	ASP	30	A	<-->	11427	CE1	PHE	456	B	2.9
49	188	OD2	ASP	30	A	<-->	11429	CZ	PHE	456	B	3.53
50	191	N	LYS	31	A	<-->	11429	CZ	PHE	456	B	3.51
51	193	CA	LYS	31	A	<-->	11429	CZ	PHE	456	B	3.85
52	195	CB	LYS	31	A	<-->	11429	CZ	PHE	456	B	3.82
53	198	CG	LYS	31	A	<-->	11929	CD1	TYR	489	B	3.63
54	201	CD	LYS	31	A	<-->	12006	OE1	GLN	493	B	3.61
55	204	CE	LYS	31	A	<-->	11864	OE1	GLN	484	B	3.17
56	204	CE	LYS	31	A	<-->	12006	OE1	GLN	493	B	3.62
57	207	NZ	LYS	31	A	<-->	11864	OE1	GLN	484	B	3.51
58	207	NZ	LYS	31	A	<-->	12005	CD	GLN	493	B	3.61
59	207	NZ	LYS	31	A	<-->	12006	OE1	GLN	493	B	2.6
60	251	CB	HIE	34	A	<-->	11366	OH	TYR	453	B	3.4
61	254	CG	HIE	34	A	<-->	11366	OH	TYR	453	B	3.45
62	254	CG	HIE	34	A	<-->	11411	CD2	LEU	455	B	3.79
63	255	ND1	HIE	34	A	<-->	11407	CD1	LEU	455	B	3.41
64	255	ND1	HIE	34	A	<-->	11411	CD2	LEU	455	B	3.32

65	256	CE1	HIE	34	A	<-->	11407	CD1	LEU	455	B	3.15
66	258	NE2	HIE	34	A	<-->	11407	CD1	LEU	455	B	3.52
67	260	CD2	HIE	34	A	<-->	11368	CE2	TYR	453	B	3.75
68	260	CD2	HIE	34	A	<-->	11365	CZ	TYR	453	B	3.8
69	260	CD2	HIE	34	A	<-->	11366	OH	TYR	453	B	2.98
70	274	CD	GLU	35	A	<-->	12007	NE2	GLN	493	B	3.83
71	275	OE1	GLU	35	A	<-->	12005	CD	GLN	493	B	3.31
72	275	OE1	GLU	35	A	<-->	12006	OE1	GLN	493	B	3.2
73	275	OE1	GLU	35	A	<-->	12007	NE2	GLN	493	B	2.61
74	301	OE2	GLU	37	A	<-->	12175	CE2	TYR	505	B	3.77
75	311	CG	ASP	38	A	<-->	11283	CE1	TYR	449	B	3.25
76	311	CG	ASP	38	A	<-->	11285	CZ	TYR	449	B	3.59
77	311	CG	ASP	38	A	<-->	11286	OH	TYR	449	B	3.13
78	312	OD1	ASP	38	A	<-->	11283	CE1	TYR	449	B	3.21
79	312	OD1	ASP	38	A	<-->	11285	CZ	TYR	449	B	3.52
80	312	OD1	ASP	38	A	<-->	11286	OH	TYR	449	B	3.3
81	312	OD1	ASP	38	A	<-->	12044	N	GLY	496	B	3.85
82	312	OD1	ASP	38	A	<-->	12046	CA	GLY	496	B	3.13
83	313	OD2	ASP	38	A	<-->	11283	CE1	TYR	449	B	2.77
84	313	OD2	ASP	38	A	<-->	11285	CZ	TYR	449	B	2.91
85	313	OD2	ASP	38	A	<-->	11286	OH	TYR	449	B	2.29
86	363	CD1	TYR	41	A	<-->	12081	CD	GLN	498	B	3.52
87	363	CD1	TYR	41	A	<-->	12082	OE1	GLN	498	B	3.23
88	365	CE1	TYR	41	A	<-->	12075	CB	GLN	498	B	3.86
89	365	CE1	TYR	41	A	<-->	12078	CG	GLN	498	B	3.66
90	365	CE1	TYR	41	A	<-->	12081	CD	GLN	498	B	3.51
91	365	CE1	TYR	41	A	<-->	12082	OE1	GLN	498	B	3.29
92	370	CE2	TYR	41	A	<-->	12124	OD1	ASN	501	B	3.88
93	367	CZ	TYR	41	A	<-->	12112	OG1	THR	500	B	3.65
94	367	CZ	TYR	41	A	<-->	12124	OD1	ASN	501	B	3.53
95	368	OH	TYR	41	A	<-->	12114	C	THR	500	B	3.43
96	368	OH	TYR	41	A	<-->	12115	O	THR	500	B	3.56
97	368	OH	TYR	41	A	<-->	12106	CB	THR	500	B	3.36
98	368	OH	TYR	41	A	<-->	12112	OG1	THR	500	B	2.52
99	368	OH	TYR	41	A	<-->	12116	N	ASN	501	B	3.58
100	368	OH	TYR	41	A	<-->	12124	OD1	ASN	501	B	3.53
101	383	CG	GLN	42	A	<-->	11286	OH	TYR	449	B	3.39
102	386	CD	GLN	42	A	<-->	11251	O	GLY	446	B	3.47
103	386	CD	GLN	42	A	<-->	11286	OH	TYR	449	B	3.46
104	386	CD	GLN	42	A	<-->	12083	NE2	GLN	498	B	3.65
105	387	OE1	GLN	42	A	<-->	11247	CA	GLY	446	B	3.85
106	387	OE1	GLN	42	A	<-->	11251	O	GLY	446	B	3.56
107	388	NE2	GLN	42	A	<-->	11250	C	GLY	446	B	3.42
108	388	NE2	GLN	42	A	<-->	11251	O	GLY	446	B	2.52
109	388	NE2	GLN	42	A	<-->	11288	CE2	TYR	449	B	3.3

110	388	NE2	GLN	42	A	<-->	11285	CZ	TYR	449	B	3.33
111	388	NE2	GLN	42	A	<-->	11286	OH	TYR	449	B	2.68
112	388	NE2	GLN	42	A	<-->	12083	NE2	GLN	498	B	3.24
113	1001	O	MET	82	A	<-->	11889	CZ	PHE	486	B	3.67
114	989	CB	MET	82	A	<-->	11885	CD1	PHE	486	B	3.7
115	989	CB	MET	82	A	<-->	11887	CE1	PHE	486	B	3.13
116	989	CB	MET	82	A	<-->	11889	CZ	PHE	486	B	3.63
117	995	SD	MET	82	A	<-->	11885	CD1	PHE	486	B	3.51
118	1012	CE1	TYR	83	A	<-->	11887	CE1	PHE	486	B	3.33
119	1012	CE1	TYR	83	A	<-->	11889	CZ	PHE	486	B	3.42
120	1012	CE1	TYR	83	A	<-->	11906	ND2	ASN	487	B	3.39
121	1017	CE2	TYR	83	A	<-->	11887	CE1	PHE	486	B	3.51
122	1014	CZ	TYR	83	A	<-->	11885	CD1	PHE	486	B	3.81
123	1014	CZ	TYR	83	A	<-->	11887	CE1	PHE	486	B	3.07
124	1014	CZ	TYR	83	A	<-->	11889	CZ	PHE	486	B	3.7
125	1014	CZ	TYR	83	A	<-->	11906	ND2	ASN	487	B	3.89
126	1015	OH	TYR	83	A	<-->	11885	CD1	PHE	486	B	3.5
127	1015	OH	TYR	83	A	<-->	11887	CE1	PHE	486	B	3.22
128	1015	OH	TYR	83	A	<-->	11897	N	ASN	487	B	3.84
129	1015	OH	TYR	83	A	<-->	11906	ND2	ASN	487	B	3.48
130	1015	OH	TYR	83	A	<-->	11934	OH	TYR	489	B	2.83
131	4962	CG	ASN	330	A	<-->	12106	CB	THR	500	B	3.78
132	4962	CG	ASN	330	A	<-->	12108	CG2	THR	500	B	3.63
133	4963	OD1	ASN	330	A	<-->	12106	CB	THR	500	B	3.76
134	4963	OD1	ASN	330	A	<-->	12108	CG2	THR	500	B	3.19
135	4964	ND2	ASN	330	A	<-->	12104	CA	THR	500	B	3.48
136	4964	ND2	ASN	330	A	<-->	12114	C	THR	500	B	3.77
137	4964	ND2	ASN	330	A	<-->	12115	O	THR	500	B	3.17
138	4964	ND2	ASN	330	A	<-->	12106	CB	THR	500	B	3.29
139	4964	ND2	ASN	330	A	<-->	12108	CG2	THR	500	B	3.68
140	5287	CA	LYS	353	A	<-->	12164	CB	TYR	505	B	3.75
141	5287	CA	LYS	353	A	<-->	12167	CG	TYR	505	B	3.41
142	5287	CA	LYS	353	A	<-->	12168	CD1	TYR	505	B	3.84
143	5287	CA	LYS	353	A	<-->	12177	CD2	TYR	505	B	3.44
144	5287	CA	LYS	353	A	<-->	12175	CE2	TYR	505	B	3.88
145	5305	C	LYS	353	A	<-->	12130	N	GLY	502	B	3.87
146	5305	C	LYS	353	A	<-->	12164	CB	TYR	505	B	3.55
147	5305	C	LYS	353	A	<-->	12167	CG	TYR	505	B	3.3
148	5305	C	LYS	353	A	<-->	12168	CD1	TYR	505	B	3.27
149	5305	C	LYS	353	A	<-->	12177	CD2	TYR	505	B	3.88
150	5305	C	LYS	353	A	<-->	12170	CE1	TYR	505	B	3.85
151	5306	O	LYS	353	A	<-->	12118	CA	ASN	501	B	3.45
152	5306	O	LYS	353	A	<-->	12128	C	ASN	501	B	3.54
153	5306	O	LYS	353	A	<-->	12120	CB	ASN	501	B	3.57
154	5306	O	LYS	353	A	<-->	12130	N	GLY	502	B	2.81

155	5306	O	LYS	353	A	<-->	12132	CA	GLY	502	B	3.64
156	5306	O	LYS	353	A	<-->	12136	O	GLY	502	B	3.67
157	5306	O	LYS	353	A	<-->	12164	CB	TYR	505	B	3.06
158	5306	O	LYS	353	A	<-->	12167	CG	TYR	505	B	3.3
159	5306	O	LYS	353	A	<-->	12168	CD1	TYR	505	B	3.35
160	5289	CB	LYS	353	A	<-->	12123	CG	ASN	501	B	3.75
161	5289	CB	LYS	353	A	<-->	12124	OD1	ASN	501	B	3.81
162	5289	CB	LYS	353	A	<-->	12125	ND2	ASN	501	B	3.89
163	5289	CB	LYS	353	A	<-->	12164	CB	TYR	505	B	3.83
164	5295	CD	LYS	353	A	<-->	12050	O	GLY	496	B	3.54
165	5295	CD	LYS	353	A	<-->	12082	OE1	GLN	498	B	3.56
166	5295	CD	LYS	353	A	<-->	12123	CG	ASN	501	B	3.85
167	5295	CD	LYS	353	A	<-->	12124	OD1	ASN	501	B	3.59
168	5295	CD	LYS	353	A	<-->	12125	ND2	ASN	501	B	3.52
169	5298	CE	LYS	353	A	<-->	12050	O	GLY	496	B	3.45
170	5298	CE	LYS	353	A	<-->	12082	OE1	GLN	498	B	3.66
171	5301	NZ	LYS	353	A	<-->	12046	CA	GLY	496	B	3.56
172	5301	NZ	LYS	353	A	<-->	12049	C	GLY	496	B	3.39
173	5301	NZ	LYS	353	A	<-->	12050	O	GLY	496	B	2.52
174	5301	NZ	LYS	353	A	<-->	12081	CD	GLN	498	B	3.59
175	5301	NZ	LYS	353	A	<-->	12082	OE1	GLN	498	B	2.72
176	5301	NZ	LYS	353	A	<-->	12083	NE2	GLN	498	B	3.6
177	5307	N	GLY	354	A	<-->	12168	CD1	TYR	505	B	3.47
178	5307	N	GLY	354	A	<-->	12170	CE1	TYR	505	B	3.65
179	5309	CA	GLY	354	A	<-->	12130	N	GLY	502	B	3.88
180	5309	CA	GLY	354	A	<-->	12168	CD1	TYR	505	B	3.83
181	5312	C	GLY	354	A	<-->	12130	N	GLY	502	B	3.37
182	5312	C	GLY	354	A	<-->	12132	CA	GLY	502	B	3.5
183	5313	O	GLY	354	A	<-->	12130	N	GLY	502	B	3.38
184	5313	O	GLY	354	A	<-->	12132	CA	GLY	502	B	3.1
185	5314	N	ASP	355	A	<-->	12130	N	GLY	502	B	3.62
186	5318	CB	ASP	355	A	<-->	12115	O	THR	500	B	3
187	5321	CG	ASP	355	A	<-->	12114	C	THR	500	B	3.8
188	5321	CG	ASP	355	A	<-->	12115	O	THR	500	B	2.81
189	5322	OD1	ASP	355	A	<-->	12115	O	THR	500	B	3.26
190	5323	OD2	ASP	355	A	<-->	12114	C	THR	500	B	3.75
191	5323	OD2	ASP	355	A	<-->	12115	O	THR	500	B	3.09
192	5323	OD2	ASP	355	A	<-->	12106	CB	THR	500	B	3.53
193	5323	OD2	ASP	355	A	<-->	12112	OG1	THR	500	B	3.64
194	5365	NH2	ARG	357	A	<-->	12106	CB	THR	500	B	3.24
195	5365	NH2	ARG	357	A	<-->	12112	OG1	THR	500	B	3.29
196	5365	NH2	ARG	357	A	<-->	12108	CG2	THR	500	B	3.53
197	5821	O	ALA	386	A	<-->	12173	OH	TYR	505	B	3.74

***Table** 7.7. List of atom-atom interactions (salt bridges) across protein-protein interface in S protein (DM)–ACE2 complex from PDBsum server*

ACE2							S protein (DM)					
Sl.no.	Atom no.	Atom name	Res name	Res no.	Chain	**salt bridges**	Atom no.	Atom name	Res name	Res no.	Chain	Distance
1	188	OD2	ASP	30	A	<-->	10810	NZ	LYS	417	B	2.52

7.4.1.5. Binding Free energy and per residue energy decomposition (PRED) analysis.

Binding free energies of the S protein(WT)-ACE2 and S protein(DM)-ACE2 complexes were calculated from the last 10 ns of the MD simulation once the system reached equilibrium using MM-PBSA/GBSA approach. The values here represent only the relative binding free energy rather than absolute or total binding energy, as MM-PBSA/GBSA approach uses a continuum solvent approach to determine the binding free energies of a system. The binding free energies determined for the wild type and mutant complexes and the energy terms were summarized in **Tables 7.8 and 7.9**. From the **Tables 7.8 and 7.9**, it can be seen that S protein(DM)-ACE2 complex (GB_{TOT} = -47.09 kcal/mol, ΔG_{bind} (GBSA)= -43.27 kcal/mol, PB_{TOT}= -19.93 kcal/mol, ΔG_{bind} (PBSA)= -16.11 kcal/mol) was energetically more favourable than the S protein(WT)-ACE2 complex (GB_{TOT} =-31.79 kcal/mol, ΔG_{bind} (GBSA)= -28.23 kcal/mol, PB_{TOT}= -6.33 kcal/mol, ΔG_{bind} (PBSA)= -2.77 kcal/mol). **Tables 7.8 and 7.9** show that all of the BFE components contributed to S protein and ACE2 binding to form the S protein(WT/DM)-ACE2 complex.

***Table 7.8.** Binding free energies (kcal/mol) and its components of S protein(WT)-ACE2 and S protein(DM)-ACE2 complexes obtained using MM-GBSA approach.*

	$\Delta G_{(S\ protein(WT)-ACE2)}$ - [$\Delta G_{S\ protein(WT)}$+ ΔG_{ACE2}] (kcal/mol)		**$\Delta G_{(S\ protein(DM)-ACE2)}$ - [$\Delta G_{S\ protein(DM)}$+ ΔG_{ACE2}] (kcal/mol)**	
	average	**std. dev. (±)**	**average**	**std. dev. (±)**
VDW	-86.32	3.93	-98.83	4.44
ELE	-676.23	14.17	-1151.78	17.92
GB	760.56	12.20	1208.30	17.07
GBSUR	-13.80	0.14	-14.78	0.43
GAS	-762.56	11.45	-1250.61	17.38
GBSOL	714.76	12.22	1213.52	16.98
GBTOT	**-31.79**	2.32	**-47.09**	5.01
TΔS	-3.56	0.33	-3.82	2.43
ΔG_{bind}	**-28.23**		**-43.27**	

Table 7.9. *Binding free energies (kcal/mol) and its components of S protein(WT)-ACE2 and S protein(DM)-ACE2 complexes obtained using MM-PBSA approach*

	$\Delta G_{(S\ protein(WT)-ACE2)} - [\Delta G_{S\ protein(WT)} + \Delta G_{ACE2}]$ (kcal/mol)		**$\Delta G_{(S\ protein(DM)-ACE2)} - [\Delta G_{S\ protein(DM)} + \Delta G_{ACE2}]$ (kcal/mol)**	
	Average	std. dev. (±)	average	std. dev. (±)
VDW	-86.32	3.93	-98.83	4.44
ELE	-676.23	14.17	-1151.78	17.92
PB	670.65	13.30	1163.82	17.03
ENPOLAR	-68.21	0.89	-72.99	2.06
EDISPER	141.78	1.26	139.84	2.51
GAS	-762.56	11.45	-1250.61	17.38
PBSOL	768.22	13.04	1230.67	17.33
PBTOT	**-6.33**	2.45	**-19.93**	6.83
TΔS	-3.56	0.33	-3.82	2.43
ΔG_{bind}	**-2.77**		**-16.11**	

PRED values were also calculated for gaining insights into the contribution of each animo acid residues of the overall protein-protein interaction. In this analysis, the total binding energy was decomposed into residues to identify key residues for ACE2 binding to S protein (WT/DM). Essential residues with the binding energy value below -1.00 kcal/mol were shown in **Figures 7.9** and **7.10**. The residues that contribute highest energy for S protein are GLN498, GLN493, LYS417, ASN487, PHE486, TYR505, TYR449, TYR489, PHE456, GLY496, ASN501, and ASN487, while in S protein (DM) come from the residues LYS417, GLN498, GLN493, TYR505, PHE486, TYR449, TYR489, PHE456, ALA475, PHE490, LEU492, and LEU455.

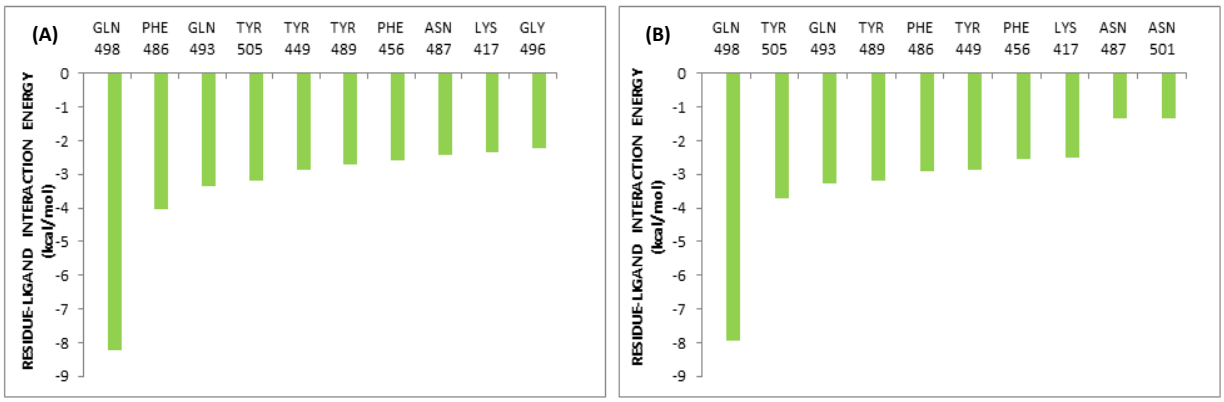

Figure 7.9. *Decomposition of binding free energy (kcal/mol) on per residue basis for ACE2 binding to S protein (WT) obtained using* ***(A)*** *MM-GBSA approach* ***(B)*** *MM-PBSA approach.*

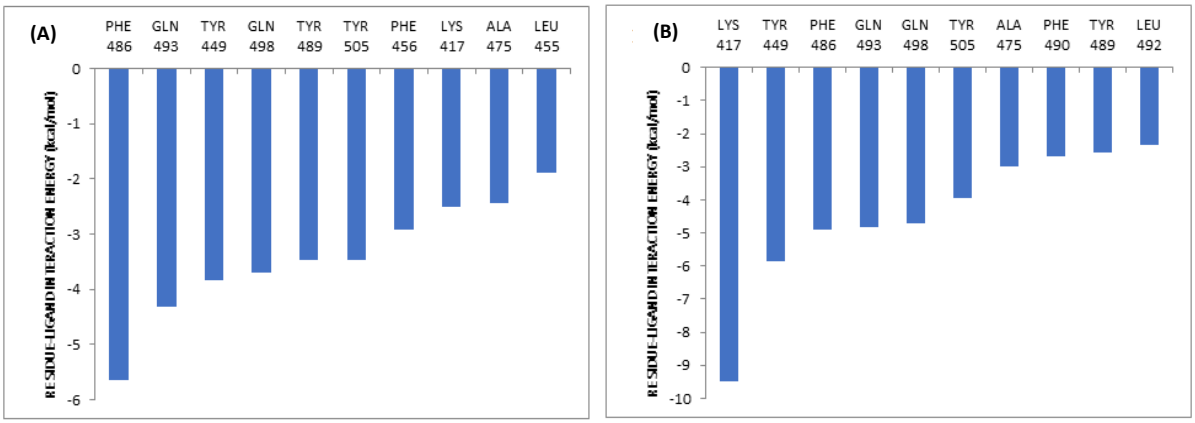

Figure 7.10. *Decomposition of binding free energy (kcal/mol) on per residue basis for ACE2 binding to S protein (DM) obtained using* ***(A)*** *MM-GBSA approach* ***(B)*** *MM-PBSA approach.*

Discussion: The results of the various analysis performed in this study suggest that the double mutant (L452R and E484Q) of the SARS-CoV-2 spike protein exhibits enhanced stability as shown by a reduced RMSD and RMSF values for the mutant complex, particularly in and around the mutated residues. It was seen the the mutated residues along with few residues around it attained higher stabilty in the mutated complex.

Additionally, binding free energy and PRED analysis reflects light on the binding of the RBD to the ACE2 receptor in both the complex and results showed that the mutated complex had significantly more favorable energetics than the wild-type and the residues in and around the mutation have the highest contribution to the total binding energy hence supporting the possibility of increased infectivity in the mutated complex. The structural and energetic insights from this analysis can aid in designing new ligands or inhibitors by highlighting key mutation-site residues that serve as critical hotspots for increase stability and binding affinity.

7.5. Conclusion:

There is a lack of adequate data to say whether the double mutant variant (B.1.617) of the SARS-CoV-2 virus is bringing a severer form of COVID-19 illness compared to the one witnessed during the first wave of the pandemic. It is unclear if the increased fatality is connected to the double mutant being deadlier or the inflated infections volume. The present study demonstrates the effect of this double mutant (E484Q and L452R) on SARS-CoV-2 RBD towards its binding with the ACE2 by employing Molecular dynamics and other computational approaches. From the MD simulation of S protein(WT)-ACE2 and S protein(DM)-ACE2 complexes, we found the double mutant (E484Q and L452R) causes extensive

structural changes in the mutation region of spike protein in S protein(DM)-ACE2 complex. From the RMSD, RMSF, and number of inter-molecular hydrogen bond analyses, we found S protein(DM)-ACE2 complex to have enhanced stability than the S protein(WT)-ACE2 complex. The number of non-bonded contacts as also higher in S protein(DM)-ACE2 complex. From the binding free energy calculations of the S protein(WT)-ACE2 and S protein(DM)-ACE2 complexes, we found that the double mutant complex's affinity between S protein and ACE2 is higher. The overall stability of the S protein(DM)-ACE2 complex and the increased affinity between S protein (DM) and ACE2 may result in higher virulence of the double mutant strain than its wild-type strain. The salient interactions that we have reported across the S protein and ACE2 in the wild type and the double mutant complexes could be used to design novel inhibitors against the newly emerging coronavirus strains.

7.6. Bibliography:

[1]. Han, H. J., Nwagwu, C., Anyim, O., Ekweremadu, C., and Kim, S. COVID-19 and cancer: From basic mechanisms to vaccine development using nanotechnology. *International Immunopharmacology,* 90: 107247, 2021. https://doi.org/10.1016/j.intimp.2020.107247

[2]. Lu, R., Zhao, X., Li, J., Niu, P., Yang, B., Wu, H., Wang, W., Song, H., Huang, B., Zhu, N., Bi, Y., Ma, X., Zhan, F., Wang, L., Hu, T., Zhou, H., Hu, Z., Zhou, W., Zhao, L., Chen, J., Meng, Y., Wang, J., Lin, Y., Yuan, J., Xie, Z., Ma, J., Liu, W. J., Wang, D., Xu, W., Holmes, E. C., Gao, G. F., Wu, G., Chen, W., Shi, W., and Tan, W. Genomic characterisation and epidemiology of 2019 novel coronavirus: Implications for virus origins and receptor binding. *The Lancet,* 395(10224): 565–574, 2020. https://doi.org/10.1016/S0140-6736(20)30251-8

[3]. Zhu, N., Zhang, D., Wang, W., Li, X., Yang, B., Song, J., Zhao, X., Huang, B., Shi, W., Lu, R., Niu, P., Zhan, F., Ma, X., Wang, D., Xu, W., Wu, G., Gao, G. F., and Tan, W. A novel coronavirus from patients with pneumonia in China, 2019. *New England Journal of Medicine,* 382*(*8): 727–733, 2020. https://doi.org/10.1056/NEJMoa2001017

[4]. Whittaker, G. R., Daniel, S., and Millet, J. K. Coronavirus entry: How we arrived at SARS-CoV-2. *Current Opinion in Virology,* 47*:* 113–120, 2021. https://doi.org/10.1016/j.coviro.2021.02.006

[5]. Bestle, D., Heindl, M. R., Limburg, H., Van Lam, T., Pilgram, O., Moulton, H., Stein, D. A., Hardes, K., Eickmann, M., Dolnik, O., Rohde, C., Klenk, H. D., Garten, W., Steinmetzer, T., & Böttcher-Friebertshäuser, E. TMPRSS2 and furin are both essential for proteolytic activation of

SARS-CoV-2 in human airway cells. *Life Science Alliance*, 3(9): e202000786, 2020. https://doi.org/10.26508/lsa.202000786

[6]. Hoffmann, M., Kleine-Weber, H., and Pöhlmann, S. A multibasic cleavage site in the spike protein of SARS-CoV-2 is essential for infection of human lung cells. *Molecular Cell,* 78*(*4): 779–784, 2020. https://doi.org/10.1016/j.molcel.2020.04.022

[7]. Papa, G., Mallery, D. L., Albecka, A., Welch, L. G., Cattin-Ortolá, J., Luptak, J., Paul, D., McMahon, H. T., Goodfellow, I. G., Carter, A., Munro, S., and James, L. C. Furin cleavage of SARS-CoV-2 spike promotes but is not essential for infection and cell-cell fusion. *PLOS Pathogens,* 17*(*1): e1009246, 2021. https://doi.org/10.1371/journal.ppat.1009246

[8]. Xia, X. Domains and functions of spike protein in SARS-CoV-2 in the context of vaccine design. *Viruses,* 13*(*1): 109, 2021. https://doi.org/10.3390/v13010109

[9]. Hoffmann, M., Kleine-Weber, H., Schroeder, S., Krüger, N., Herrler, T., Erichsen, S., Schiergens, T. S., Herrler, G., Wu, N.-H., Nitsche, A., Müller, M. A., Drosten, C., and Pöhlmann, S. SARS-CoV-2 cell entry depends on ACE2 and TMPRSS2 and is blocked by a clinically proven protease inhibitor. *Cell,* 181*(*2): 271–280.e8: 2020. https://doi.org/10.1016/j.cell.2020.02.052

[10]. Tsai, M. S., Yang, Y. H., Lin, Y. S., Chang, G. H., Hsu, C. M., Yeh, R. M., Shu, L. H., Cheng, Y. C., Liu, H. T., Wu, Y. H., Wu, Y. H., Shen, R. C., and Wu, C. Y. GB-2 blocking the interaction between ACE2 and wild-type and mutant spike protein of SARS-CoV-2. *Biomedicine & Pharmacotherapy,* 142: 112011, 2021. https://doi.org/10.1016/j.biopha.2021.112011

[11]. Millet, J. K., and Whittaker, G. R. Host cell entry of Middle East respiratory syndrome coronavirus after two-step, furin-mediated activation of the spike protein. *Proceedings of the National Academy of Sciences,* 111*(*42): 15214–15219, 2014. https://doi.org/10.1073/pnas.1407087111

[12]. Tortorici, M. A., and Veesler, D. Structural insights into coronavirus entry. *Advances in Virus Research,* 105: 93–116, 2019, https://doi.org/10.1016/bs.aivir.2019.08.002

[13]. Gan, H. H., Twaddle, A., Marchand, B., and Gunsalus, K. C. Structural modeling of the SARS-CoV-2 spike/human ACE2 complex interface can identify high-affinity variants associated with increased transmissibility. *Journal of Molecular Biology, 433*(17): 167051, 2021.https://doi.org/10.1016/j.jmb.2021.167051

[14]. Cherian, S., Potdar, V., Jadhav, S., Yadav, P., Gupta, N., Das, M., Das, S., Agarwal, A., Singh, S., Abraham, P., Panda, S., Mande, S., Swarup, R., Bhargava, B., Bhushan, R., NIC team, and ICMR Consortium. Convergent evolution of SARS-CoV-2 spike mutations, L452R, E484Q and P681R, in the second wave of COVID-19 in Maharashtra, India. *bioRxiv*, 2021. https://doi.org/10.1101/2021.04.22.440932

[15]. Ferreira, I. A. T. M., Kemp, S. A., Datir, R., Saito, A., Meng, B., Rakshit, P., Takaori-Kondo, A., Kosugi, Y., Uriu, K., Kimura, I., Shirakawa, K., Abdullahi, A., Agarwal, A., Ozono, S., Tokunaga, K., Sato, K., Gupta, R. K., CITIID-NIHR BioResource COVID-19 Collaboration, ISARIC4C, G2P-Japan Consortium, and The Genotype to Phenotype Japan Consortium. (2021). SARS-CoV-2 B.1.617 mutations L452R and E484Q are not synergistic for antibody evasion. *The Journal of Infectious Diseases,* 224(6), 989–994. https://doi.org/10.1093/infdis/jiab368

[16]. Zhang, L., Huynh, T., and Luan, B. *In silico* assessment of antibody drug resistance to bamlanivimab of SARS-CoV-2 variant B.1.617. *bioRxiv*, 2021. https://doi.org/10.1101/2021.05.12.443826

[17]. Berman, H. M., Westbrook, J., Feng, Z., Gilliland, G., Bhat, T. N., Weissig, H., Shindyalov, I. N., and Bourne, P. E. The Protein Data Bank. *Nucleic Acids Research,* 28(1): 235–242, 2000. https://doi.org/10.1093/nar/28.1.235

[18]. Pettersen, E. F., Goddard, T. D., Huang, C. C., Couch, G. S., Greenblatt, D. M., Meng, E. C., and Ferrin, T. E. UCSF Chimera—A visualization system for exploratory research and analysis. *Journal of Computational Chemistry, 25*(13): 1605–1612, 2004. https://doi.org/10.1002/jcc.20084

[19]. Case, D. A., Betz, R. M., Cerutti, D. S., Cheatham III, T. E., Darden, T. A., Duke, R. E., Giese, T. J., Gohlke, H., Goetz, A. W., Homeyer, N., Izadi, S., Janowski, P., Kaus, J., Kovalenko, A., Lee, T. S., LeGrand, S., Li, P., Lin, C., Luchko, T., Luo, R., Madej, B., Mermelstein, D., Merz, K. M., Monard, G., Nguyen, H., Nguyen, H. T., Omelyan, I., Onufriev, A., Roe, D. R., Roitberg, A., Sagui, C., Simmerling, C. L., Smith, W. M. B., Swails, J., Walker, R. C., Wang, J., Wolf, R. M., Wu, X., Xiao, L., and Kollman, P. A. *Amber 2016*. University of California, San Francisco, 2016.

[20]. Maier, J. A., Martinez, C., Kasavajhala, K., Wickstrom, L., Hauser, K. E., and Simmerling, C. ff14SB: Improving the accuracy of protein side chain and backbone parameters from ff99SB. *Journal of Chemical Theory and Computation,* 11(8): 3696–3713, 2015. https://doi.org/10.1021/acs.jctc.5b00255

[21]. Jorgensen, W. L., Chandrasekhar, J., Madura, J. D., Impey, R. W., and Klein, M. L. Comparison of simple potential functions for simulating liquid water. *The Journal of Chemical Physics,* 79(2): 926–935, 1983. https://doi.org/10.1063/1.445869

[22]. Yoo, S., and Xantheas, S. S. Communication: The effect of dispersion corrections on the melting temperature of liquid water. *The Journal of Chemical Physics,* 134(12): 121105, 2011. https://doi.org/10.1063/1.3573375

[23]. Loncharich, R. J., Brooks, B. R., and Pastor, R. W. Langevin dynamics of peptides: The frictional dependence of isomerization of N-acetylalanyl-N′-methylamide. *Biopolymers,* 32(5): 523–535, 1992. https://doi.org/10.1002/bip.360320508

[24]. Darden, T., York, D., and Pedersen, L. Particle mesh Ewald: An N·log(N) method for Ewald sums in large systems. *The Journal of Chemical Physics,* 98(12): 10089–10092, 1993. https://doi.org/10.1063/1.464397

[25]. Salomon-Ferrer, R., Götz, A. W., Poole, D., Le Grand, S., and Walker, R. C. Routine microsecond molecular dynamics simulations with AMBER on GPUs. 2. Explicit solvent particle mesh Ewald. *Journal of Chemical Theory and Computation,* 9(9): 3878–3888, 2013. https://doi.org/10.1021/ct400314y

[26]. Ryckaert, J.-P., Ciccotti, G., and Berendsen, H. J. C. Numerical integration of the Cartesian equations of motion of a system with constraints: Molecular dynamics of *n*-alkanes. *Journal of Computational Physics,* 23(3): 327–341, 1977. https://doi.org/10.1016/0021-9991(77)90098-5

[27]. Krautler, V., van Gunsteren, W. F., and Hünenberger, P. H. A fast SHAKE algorithm to solve distance constraint equations for small molecules in molecular dynamics simulations. *Journal of Computational Chemistry,* 22(5): 501–508, 2001. https://doi.org/10.1002/1096-987X(20010415)22:53.0.CO;2-V

[28]. Berendsen, H. J., Postma, J. V., van Gunsteren, W. F., DiNola, A., and Haak, J. R. Molecular dynamics with coupling to an external bath. *The Journal of Chemical Physics,* 81(8): 3684–3690, 1984. https://doi.org/10.1063/1.448118

[29]. Tchesnokova, V., Kulakesara, H., Larson, L., Bowers, V., Rechkina, E., Kisiela, D., Sledneva, Y., Choudhury, D., Maslova, I., Deng, K., Kutumbaka, K., Geng, H., Fowler, C., Greene, D., Ralston, J., Samadpour, M., and Sokurenko, E. Acquisition of the L452R mutation in the ACE2-

binding interface of spike protein triggers recent massive expansion of SARS-CoV-2 variants. *Journal of Clinical Microbiology,* 59(11): e00921-21, 2021. https://doi.org/10.1128/jcm.00921-21

[30]. Laskowski, R. A., Hutchinson, E. G., Michie, A. D., Wallace, A. C., Jones, M. L., and Thornton, J. M. PDBsum: A web-based database of summaries and analyses of all PDB structures. *Trends in Biochemical Sciences,* 22(12): 488–490, 1997. https://doi.org/10.1016/s0968-0004(97)01140-7

[31]. Case, D. A. Normal mode analysis of protein dynamics. *Current Opinion in Structural Biology,* 4(2): 285–290, 1994. https://doi.org/10.1016/S0959-440X(94)90321-2

[32]. Chen, F., Liu, H., Sun, H., Pan, P., Li, Y., Li, D., and Hou, T. Assessing the performance of the MM/PBSA and MM/GBSA methods. 6. Capability to predict protein–protein binding free energies and re-rank binding poses generated by protein–protein docking. *Physical Chemistry Chemical Physics,* 18(30): 22129–22139, 2016. https://doi.org/10.1261/rna.065896.118

[33]. Genheden, S., and Ryde, U. The MM/PBSA and MM/GBSA methods to estimate ligand-binding affinities. *Expert Opinion on Drug Discovery,* 10(5): 449–461, 2015. https://doi.org/10.1517/17460441.2015.1032936

[34]. Sun, H., Duan, L., Chen, F., Liu, H., Wang, Z., Pan, P., Zhu, F., Zhang, J. Z. H., and Hou, T. Assessing the performance of MM/PBSA and MM/GBSA methods. 7. Entropy effects on the performance of end-point binding free energy calculation approaches. *Physical Chemistry Chemical Physics,* 20(22): 14450–14460, 2018. https://doi.org/10.1039/c7cp07623a

[35]. Wang, E., Sun, H., Wang, J., Wang, Z., Liu, H., Zhang, J. Z. H., and Hou, T. End-point binding free energy calculation with MM/PBSA and MM/GBSA: Strategies and applications in drug design. *Chemical Reviews,* 119(16): 9478–9508, 2019. https://doi.org/10.1021/acs.chemrev.9b00055